Electronic Supplementary Material (ESI) for Environmental Science: Nano.
This journal is © The Royal Society of Chemistry 2022

Electronic Supplementary Information

Simultaneously enhanced photocatalytic cleanup of Cr(VI) and tetracycline via $ZnIn_2S_4$ nanoflakes-decorated 24-faceted concave MIL-88B(Fe) polyhedron S-scheme system

Qingling Huang,[a] Jianqiang Hu,[a,b,d*] Yingfei Hu,[c] Jianchao Liu,[e] Jiale He,[a] Guobing Zhou,[a] Na Hu,[a,d] Zhen Yang,[a*] Yongcai Zhang,[f] Yong Zhou [b*] and Zhigang Zou[b]

[a] Institute of Advanced Materials (IAM), Key Lab of Fluorine and Silicon for Energy Materials and Chemistry of Ministry of Education, College of Chemistry and Chemical Engineering, Jiangxi Normal University, Nanchang 330022, P. R. China.

[b] National Laboratory of Solid State Microstructures, Collaborative Innovation Center of Advanced Microstructures, School of Physics, Nanjing University, Nanjing 210093, P. R. China.

[c] School of Materials Engineering, Jinling Institute of Technology, Nanjing 211169, P. R. China.

[d] State-Province Joint Engineering Laboratory of Zeolite Membrane Materials, Jiangxi Normal University, Nanchang 330022, P. R. China.

[e] National Engineering Research Center for Carbohydrate Synthesis, Jiangxi Normal University, Nanchang 330022, P. R. China.

[f] School of Chemistry and Chemical Engineering, Yangzhou University, Yangzhou, 225009, P. R. China

* Corresponding authors:

E-mail addresses: hujq@jxnu.edu.cn (J. Hu), yangzhen@jxnu.edu.cn (Z. Yang) and zhouyong1999@nju.edu.cn (Y. Zhou).

1. Experimentail

1.1 Chemicals and materials. Iron(III) chloride hexahydrate ($FeCl_3 \cdot 6H_2O$), 1, 4-benzenedicarboxylic acid (H_2BDC), N,N-dimethylformamide (DMF), ethanol absolute (AR) were purchased from Sinopharm Chemical Reagent Co., Ltd. Zinc acetate dehydrate ($Zn(Ac)_2 \cdot 2H_2O$), Indium chloride ($InCl_3$), ethylene glycol (EG) and thiacetamide (TAA) were obtained from Aladdin Industrial corporation. All chemicals were used as received, unless otherwise stated. Deionized water was prepared with a Milli-Q purity system (18.2 MΩ).

1.2 Characterizations. X-ray powder diffraction (XRD) patterns of the obtained samples were analysed using a Bruker D8 Advance diffractometer with Cu Kα radiation (λ = 0.15406 nm), and the data were gathered in the 2θ range of 10-80° at a step size of 0.02°. The microscopic morphology and structure of the samples were examined using the field-emission scanning electron microscopy (FE-SEM, Nova Nanosem 200 system operated at an acceleration voltage of 15 kV) and transmission electron microscopy (TEM, JEOL-3010 instrument.). X-ray photoelectron spectroscopy (XPS) surveys were performed by using a spectrometer from Kratos Axis Ultradld, using Mono Al Kα (1486.71eV) radiation at a power of 120 W (8 mA, 15 kV). All binding energies were referenced to the C 1s peak (284.8 eV) arising from adventitious carbon. UV-vis diffuse reflectance spectra were acquired in a UV-vis spectrophotometer (UV-2550, Shimadzu, Japan), where fine $BaSO_4$ powder was used as a reflectance standard. The steady-state photoluminescence (PL) spectra were obtained via a FLS980 Series of Fluorescence Spectrometers. The signal of $\cdot O_2^-$ and ·OH was detected by electron spin resonance spectroscopy (ESR) technique (EXM-10/12, Bruker, GER). The Fourier transform infrared spectra (FT-IR) of the samples were analysed by Spectrum one (Perkin ElmerInc., USA) in the range of 400-4000 cm^{-1} (reference: KBr).

1.3 Photoelectrochemical measurement. The photoelectrochemical measurements were performed via an electrochemical analyzer (CHI-660C, Shanghai Chenhua) in a typical three-electrode mode with 0.5 M Na_2SO_4 solution (pH = 6.5) as electrolyte. To fabricate the working electrodes, 20 mg of the pre-prepared sample was scattered into 950 μL of ethanol and 50 μL of Nafion solution (5 wt %) under sonication for 30 min. 50.0 μL of the prepared slurry was evenly distributed onto the surface of a FTO substrate (1.0 cm × 1.0 cm), and then dried in air at under room temperature for 12 h. A saturated Ag/AgCl electrode and a platinum (Pt) electrode were employed as the reference electrode and counter electrode, respectively. A 250 W Xenon lamp (Beijing Aulight Co., Ltd) with a UV-cut off filter ($\lambda > 420$ nm) was used as a light source. Potentials of the working electrode were shifted on a RHE (reversible hydrogen potential) scale by the formula $V_{RHE} = V_{Ag/AgCl} + V_0 + 0.05916 \times pH$, where V_{RHE} was the potential vs. a reversible hydrogen potential, $V_{Ag/AgCl}$ was the potential vs. Ag/AgCl electrode, $V_0 = 0.1976$ V at 25 °C and pH was the pH value of electrolyte. The active area of the sample was fixed as 0.28 cm^2 by using a black mask. The photocurrent of the sample was tested from the back side (electrolyte-substrate interface). Precisely, the Mott-Schottky (MS) plots were recorded with a frequency from 500-1500Hz and an amplitude of 10 mV. Transient photocurrent response (TPR) was examined under the 20s on/off chopped illumination and at a bias potential of 0.46 V vs. RHE. Electrochemical impedance spectra (EIS) measurements were made within the 0.1 Hz to 100k Hz frequency ranges by making use of alternating current voltage amplitude of 10 mV.

1.4 Photocatalytic test. The photocatalytic performance of pre-obtained samples were investigated via the reduction of Cr(VI) and degradation of TC under a 250 W Xe

lamp as the light source with a filter ($\lambda > 420$ nm). Typically, 80 mg of catalyst was dispersed into 100 mL of Cr(VI) or TC solution with a concentration of 20 $mg \cdot L^{-1}$, and then stirred in darkness for 1 h to achieve the adsorption-desorption equilibrium. Afterwards, each 10 min interval of light-illumination, 2mL of suspension was taken out and the solid catalyst was removed by cellulose acetate membranes with 0.22 μm of pore size. The photocatalytic removal of Cr(VI)/TC mixed pollutants was performed under the same conditions except for using 20 $mg \cdot L^{-1}$ Cr(VI) and TC solution. The Cr(VI) concentration was determined at 540 nm using the diphenylcarbazide method, and TC was measured at 357 nm. For the stability and recyclability experiments, the used catalyst was washed with 0.5 $mol \cdot L^{-1}$ HNO_3, ethanol and water for three times, and then dried in a freeze dryer for the next use.

1.5 The determination of reactive species. To survey the contribution of the active species in the photocatalytic oxidation of TC involved in the M88B@ZIS-10 sample, reactive species experiments were executed employing ethylene diamine tetraacetic acid (EDTA), 1,4-benzoquinone (BQ) and isopropyl alcohol (IPA) as scavengers to capture the photogenerated holes, $\cdot O_2^-$and ·OH, respectively.

1.6 LC-MS experiments. The intermediates produced in the photodegradation process of TC were ascertained by high performance liquid chromatography mass spectrometry (LC-MS) (thermo scientific Q Exactive). Mobile phase was a mixture of methyl alcohol and formic acid (0.1%) with a flow rate of 0.25 mL/min. The injection volume was 5.0 μL. The capillary temperature and probe heater temperature were 300 °C and 350 °C, respectively. The Spray Voltage was 3200 V and the range of the wavelength is 190-400 nm.

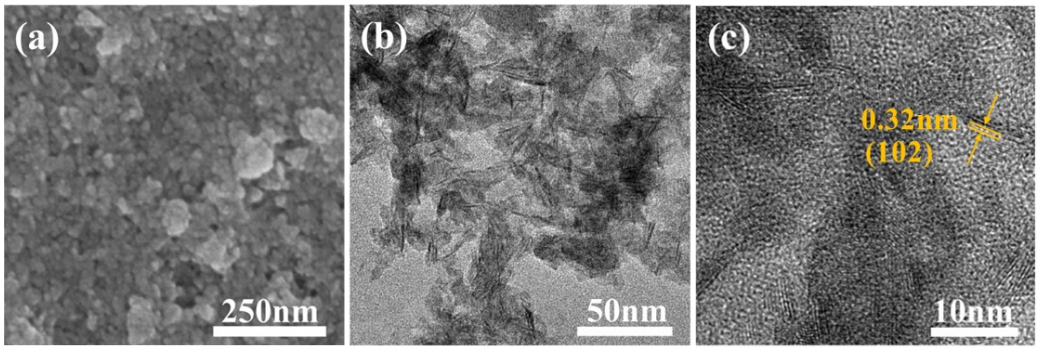

Fig. S1 (a) SEM, (b)TEM and (c) HRTEM images of the pure ZIS.

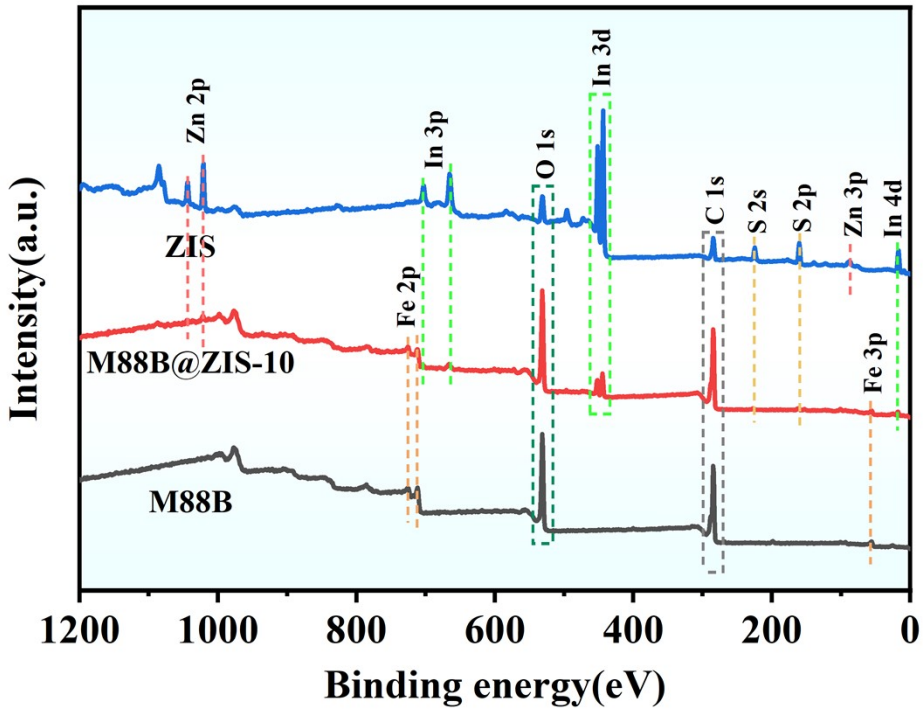

Fig. S2 XPS survey spectra of M88B, ZIS and M88B@ZIS-10.

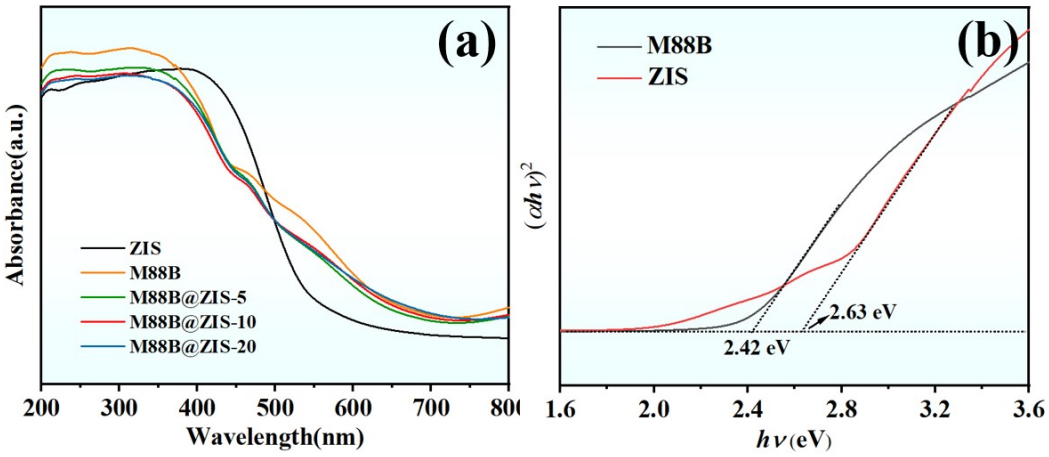

Fig. S3 (a) UV-visible absorption spectra of as-obtained samples, (b) the band edges of M88B and ZIS.

Table S1. Comparison of the photocatalytic activity of the simultaneous removal of Cr(VI) and TC over M88B@ZIS-10 with that of various reported photocatalysts.

Photocatalyst	$C_{catalyst}$ g/L	Initial Cr(VI)/TC concentration (mg/L)	Reduction rate of Cr(VI) (%)	Degradation rate of TC (%)	Time(min)	Reference
M88B@ZIS	0.8	20/20	92.46	87.14	80	This work
$AgI/BiVO_4$	0.4	20/15	70	85	100	1
$Bi_{12}O_{17}Cl_2/AgBr$	0.5	50/10	92	77	60	2
$BiPO_4/CuBi_2O_4$	0.4	30/40	60.3	92	90	3
$Cu_2O/BiOBr$	0.4	15/10	80.17	80.81	100	4
$Co_3O_4/g\text{-}C_3N_4$	0.4	15/15	92.6	81.3	150	5
$Ta_3N_5/BiOCl$	0.33	20/20	91.6	89.6	80	6
MIL-125-NH_2@BiOI	1	80/80	80	81	120	7
CoO/Bi_2WO_6	0.6	30/40	77.3	91.6	90	8

References

(S1) W. Zhao, J. Li, B. Dai, Z. Cheng, J. Xu, K. Ma, L. Zhang, N. Shenge, G. Mao, H. Wu, K. Wei, D. Y.C. Leung, *Chem. Eng. J.*, 2019, **369**, 716-725.

(S2) Z. Zhai, K. Ren, X. Zheng, Y. Chen,Y. Dong, H. Shi, *Environ. Sci.: Nano*, 2022, **9**, 1780-1793.

(S3) C. Lu, L. Wang, D. Yang, Z. Jin, X. Wang, J. Xu, Z. Li, W. Shi, W. Guan, W. Huang, *J. Alloy. Compd.*, 2022, **919**, 165849.

(S4) X. Dou, C. Zhang, H. Shi, *Sep. Purif. Technol.*, 2022, **282**, 120023.

(S5) W. Zhao, J. Li, T. T. She, S. S. Ma, Z. P. Cheng, G. X. Wang, P. S. Zhao, W. Wei, D. H. Xia, D. Y. C. Leung, J. Hazard. Mater., 2021, 402, 123839.

(S6) S. J. Li, M. J. Cai, C. C. Wang, Y. P. Liu, N. Li, P. Zhang, X. Li, *J. Mater. Sci. Technol.*, 2022, 123, 177-190.

(S7) D. Dai, J. Qiu, L. Zhang, Hong Ma, J. Yao, *J. Colloid Interface Sci.*, 2022, **607**, 933-941.

(S8) C. Lu, D. Yang, L. Wang, S. Wen, D. Cao, C. Tu, L. Gao, Y. Li, Y. Zhou, W. Huang, *J. Alloy. Compd.*, 2022, **904**, 164046.

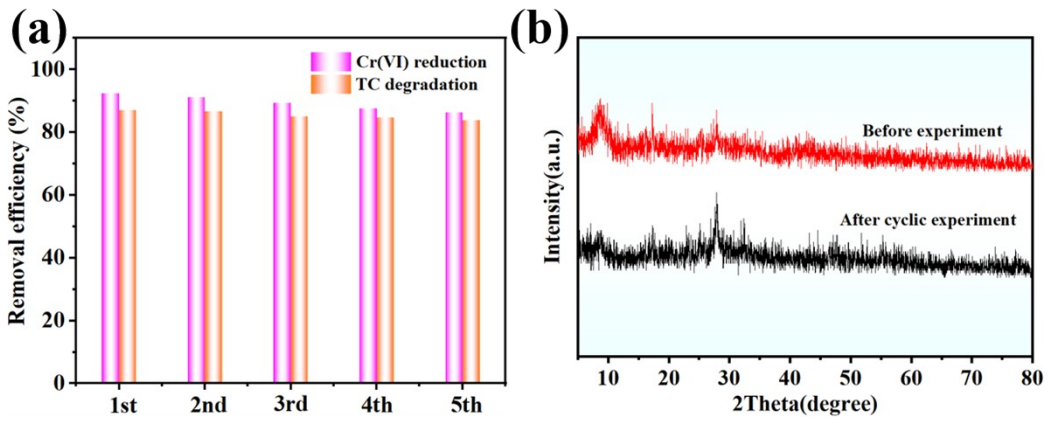

Fig. S4 (a) The recyclability of simultaneously photocatalytic removal of Cr (VI) and TC by M88B@ZIS-10, (b) XRD patterns of M88B@ZIS-10 before and after the mixed pollutant removal cyclic experiment.

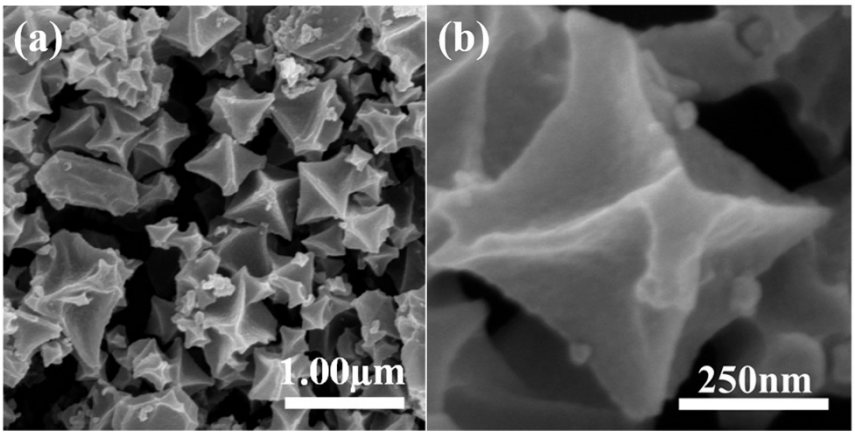

Fig. S5 SEM patterns of M88B@ZIS-10 after the mixed pollutant removal cyclic experiment.

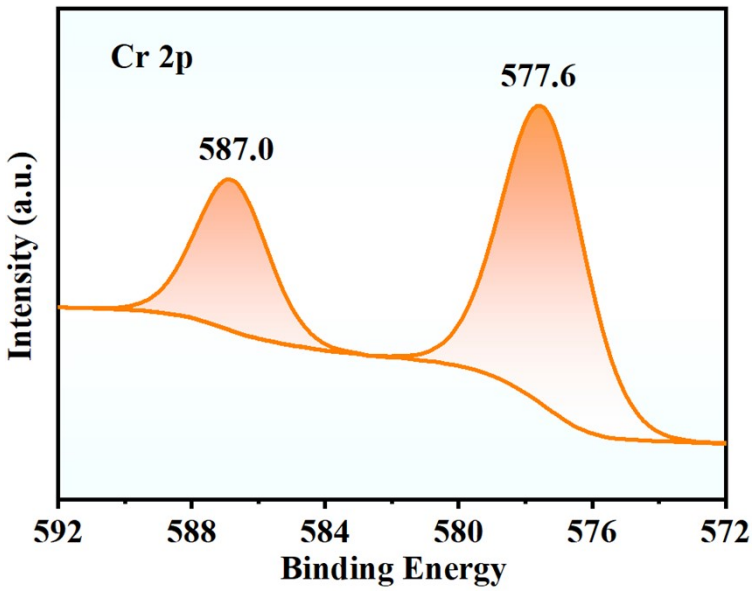

Fig. S6 High-resolution Cr 2p XPS spectrum of M88B@ZIS-10 after the mixed pollutant removal cyclic experiment.

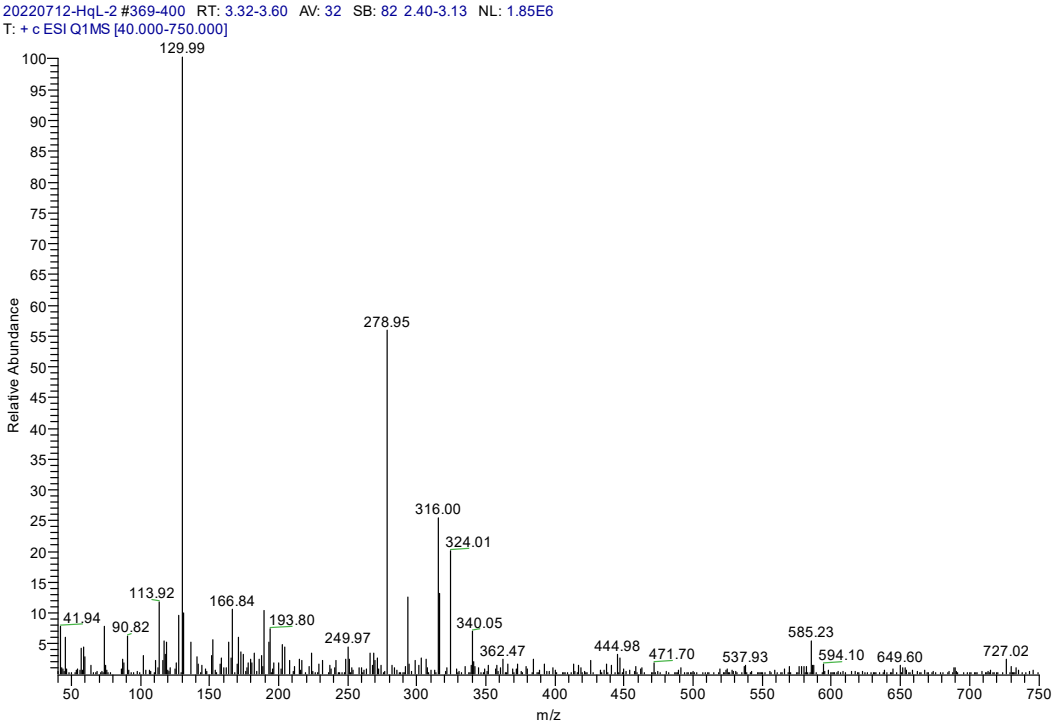

Fig. S7 Mass spectra of degradation intermediates of TC after 80 min degradation at 3.32-3.60 min retention time.

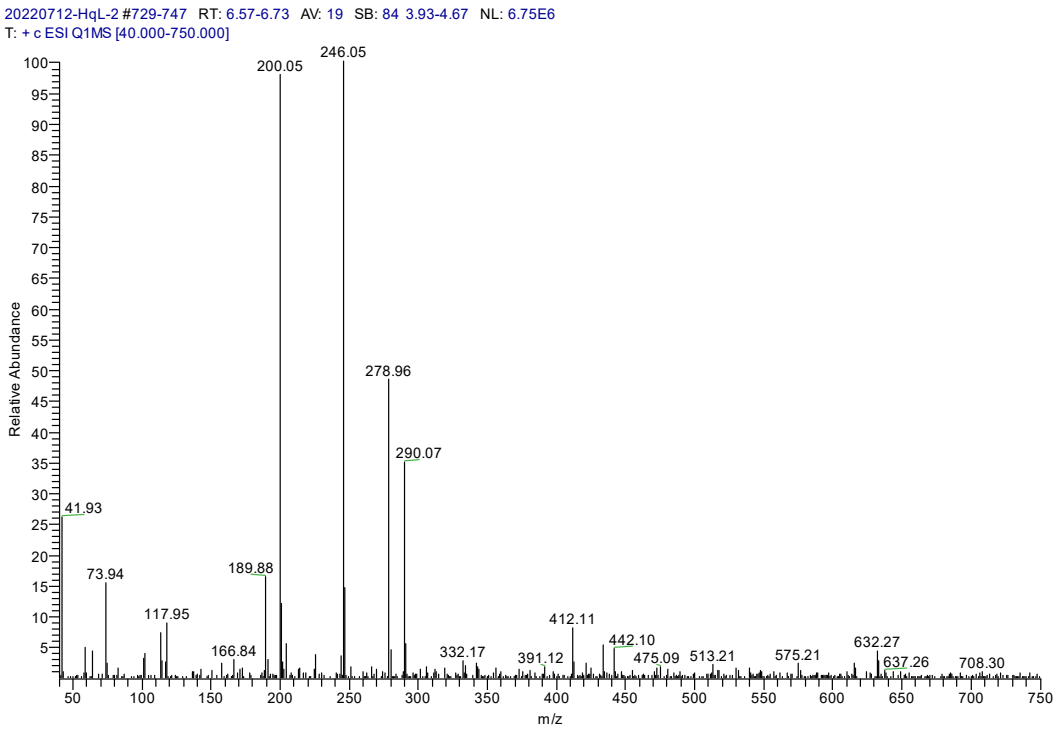

Fig. S8 Mass spectra of degradation intermediates of TC after 80 min degradation at 6.57-6.73 min retention time.

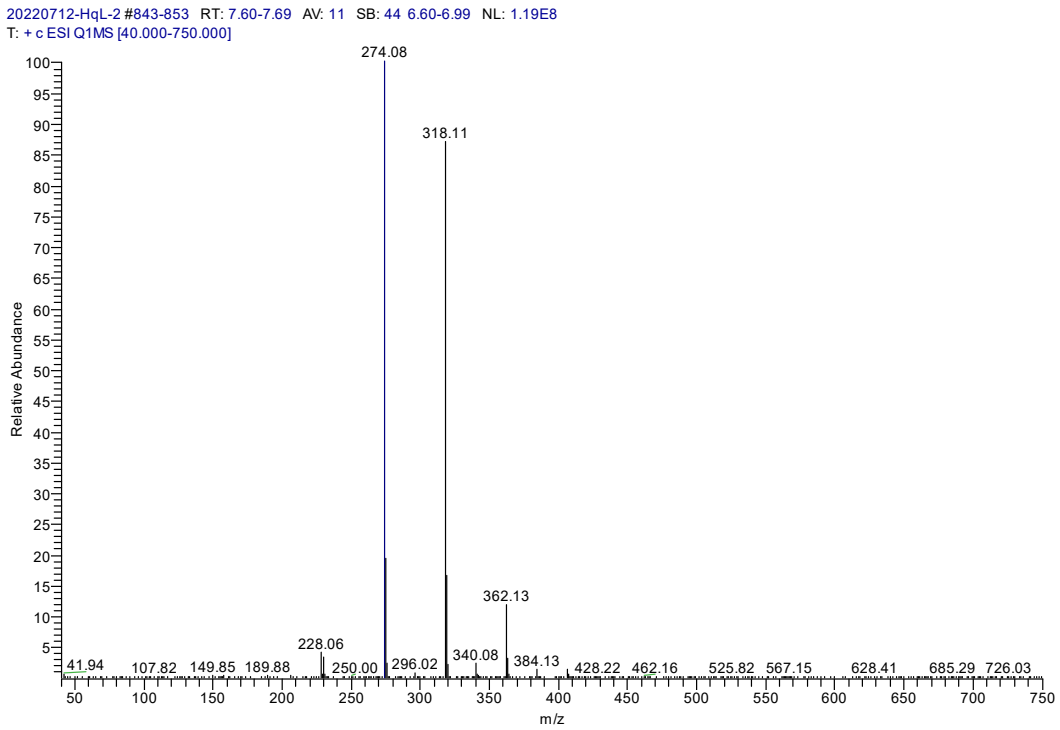

Fig. S9 Mass spectra of degradation intermediates of TC after 80 min degradation at 7.60-7.69 min retention time.

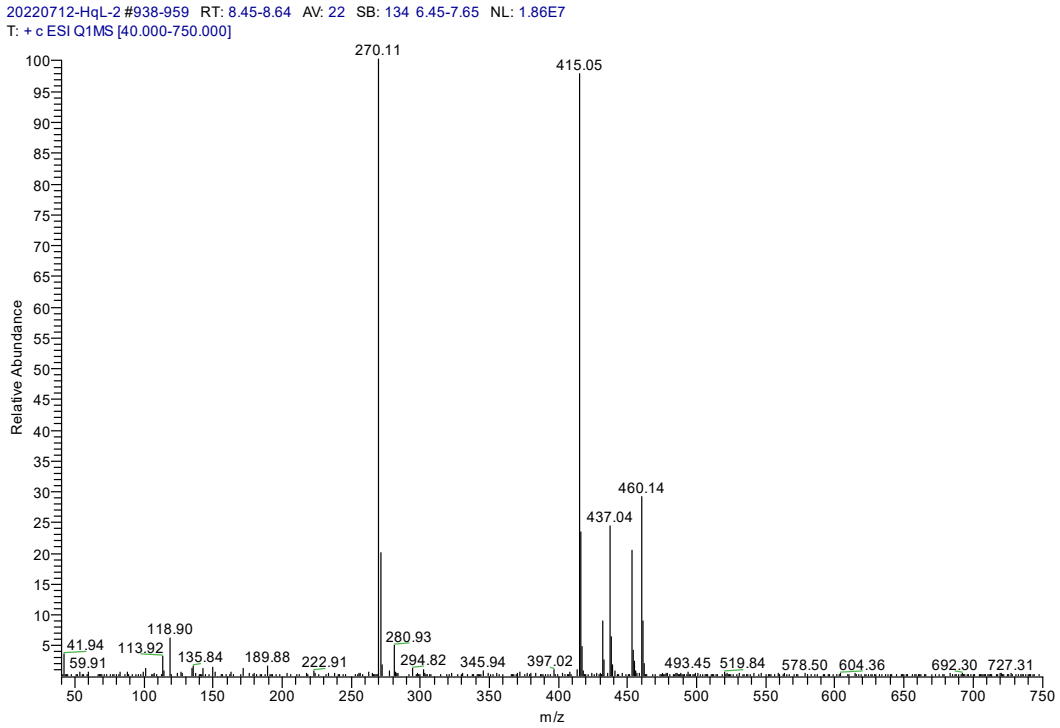

Fig. S10 Mass spectra of degradation intermediates of TC after 80 min degradation at 8.45-8.64 min retention time.

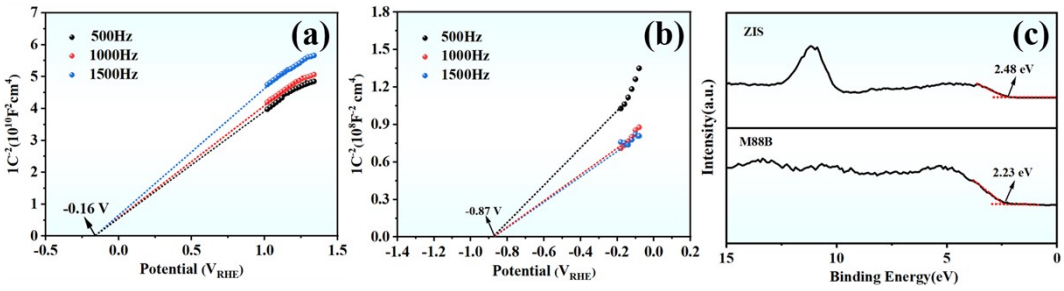

Fig. S11 Mott-Schottky plots of M88B (a), and ZIS (b), (c) the VB-XPS patterns of M88B, ZIS.